The following article appeared in Nuclear Fusion, Vol.51, No.3, March 2011, p.033006

Generation of zonal perturbations and transport barriers in plasmas
Militello F, Romanelli M, Connor J W, Hastie R J

Generation of zonal perturbations and Transport Barriers in plasmas

F. Militello, M. Romanelli, J.W. Connor and R.J. Hastie
EURATOM/CCFE Fusion Association Culham Science Centre, Abingdon, Oxon, OX14 3DB, UK

Abstract. It is shown that drift wave plasma turbulence in the electromagnetic regime can significantly affect the zonal flow dynamics and drive zonal fields. A new interpretation of the effect of the zonal fields on the zonal flow stability is given as previous analytic predictions are shown to be inadequate for accurately describing the numerical results. The zonal flow/field excitation mechanism in the electromagnetic regime can provide a possible explanation for the observed correlation between transport barrier formation and low shear rational surfaces in the plasma.

PACS numbers:

1. Introduction

Inhomogeneous laboratory and space plasmas are naturally prone to turbulence and self-organization, which often lead to the formation of long living, mesoscale structures. Examples are the solar and terrestrial dynamo mechanism, the Jovian belts, or the zonal flow and Internal Transport Barrier (ITB) formation in magnetic fusion devices. The complex interplay between these coherent structures and the turbulent fluctuations determines the relevant transport of particles and energy in the plasma [1]. As a consequence, the understanding of the mechanism leading to these phenomena is of central importance for the development of a reliable experimental fusion reactor, where the confinement of particles and energy must be extremely efficient.

In this paper, we investigate a particular case, occurring in toroidal experimental fusion devices, which is a paradigm for this mechanism. We present a detailed study of the formation of poloidally and toroidally symmetric band-like structures in the electric and poloidal magnetic field from a turbulent bath of drift waves. These perturbations induce a non-coherent shear in the fields which typically varies on spatial and temporal scales which are intermediate between the turbulence and the equilibrium, and are usually referred to as "zonal". On the other hand, this very shear is responsible for the stabilization of the turbulence and a reduction of the transport. Our main focus is the investigation of the well documented zonal flows (the electric field perturbation leads to $\mathbf{E}\times\mathbf{B}$ drifts, and therefore to a flow) and of the less studied zonal fields (the magnetic field perturbations) as the plasma becomes more and more electromagnetic.

While considerable literature has been devoted to the electrostatic limit of the zonal flows (see [1] and references therein), the study of their electromagnetic version is relatively recent, so that the first experimental observation of zonal fields was reported only fairly recently [2] (for examples from numerical simulations, see [3, 4]). Nevertheless, the problem has a great practical interest since improved energy confinement, which implies a more electromagnetic plasma, would be beneficial for next step tokamaks. More generally, a better theoretical understanding of the mechanism of generation of the zonal fields could also shed some light on the still unresolved problem of dynamo formation in astrophysical objects and laboratory plasmas. First attempts to extend the zonal flow theory to the electromagnetic regime were made by Chen *et al* [5] and by Guzdar *et al* [6, 7] using kinetic and fluid theory, respectively. In these references, the analysis is based on a coherent modulational theory (parametric instability) which assumes a narrow spectrum for the turbulence. Within this model, the zonal perturbation is generated through a four wave interaction which couples it to a single finite amplitude Drift-Alfven wave, called the "pump" wave, and two sidebands. These analytic calculations employed perturbative expansions which relied upon the assumption of a time scale separation between the pump wave and the zonal fields. Our mathematical approach follows those in [6, 7]. However, we have identified some approximations in the original perturbative technique which led to quantitatively different predictions in some parametric domains, as a comparison with our numerical solution shows. Furthermore, our model includes the effect of finite electron inertia, previously neglected in similar fluid calculations.

Finally, we propose a new interpretation of the formation of self-sustained zonal flows, which in our model can occur even in presence of small β in the neighbourhood of a low shear rational surface. Indeed, our critical transition parameter is proportional to $\sqrt{\beta}$ and inversely proportional to the parallel wavelength of the fluctuations, $k_{\|}$. This

latter feature is of extreme importance as in the vicinity of a low shear rational surface the smallness of $k_\parallel$ compensates that of $\sqrt{\beta}$. Therefore, in these special locations, the transition parameter can be extremely large and can easily exceed the critical transition threshold of order unity. This observation (which despite its simplicity is not present in previous similar works) can provide a theoretical justification for the puzzling experimental correlations between ITBs and resonant surfaces [8].

2. Model

Our study relies on a reduced Drift Fluid model which is well suited to describe the behaviour of a quasi-neutral plasma in a large aspect ratio tokamak with weak flows and temperature gradients ($T_e \cong const$, $T_i \cong 0$) and small but finite β (the ratio between kinetic and magnetic pressure). For the sake of simplicity, we restrict our attention to a slab configuration. Although the geometry is likely to play a role in determining the details of the zonal perturbations, we believe that it does not modify our overall picture. Another key approximation is the assumption that the magnetic shear is extremely small, so that the parallel component of the wave vector can be assumed roughly constant. Our model employs an ideal and reduced version of the normalized fluid equations described in [9]:

$$\partial U/\partial t + [\phi, U] = [J, \psi] + \frac{\partial J}{\partial z}, \tag{1}$$

$$\partial \chi/\partial t + [\phi, \chi] + \frac{\partial \phi}{\partial z} = [n, \psi] + \frac{\partial n}{\partial z}, \tag{2}$$

$$\partial n/\partial t + [\phi, n] = \rho^2 \left([J, \psi] + \frac{\partial J}{\partial z} \right). \tag{3}$$

with $\chi = \psi - d_e^2 \nabla_\perp^2 \psi$ and d_e the collisionless skin depth.

Three normalized fields are evolved: the density, n, the electric potential, ϕ, and the magnetic flux, ψ. The normalized magnetic field can be represented as: $\mathbf{B} = \mathbf{e}_z - \mathbf{e}_z \times \nabla_\perp \psi$, where $\mathbf{e}_z$ is a unity vector along the confining magnetic field, B_z. Assuming negligible parallel ion velocity and within a cold ion approximation, the normalized ion velocity is given by the $\mathbf{E} \times \mathbf{B}$ drift, so that: $\mathbf{V} = \mathbf{e}_z \times \nabla_\perp \phi$. With these definitions, $U = \nabla_\perp^2 \phi$ represents the plasma vorticity, while $J = -\nabla_\perp^2 \psi$ is the current density in the "toroidal" direction (i.e. along $\mathbf{e}_z$). Finally, the Poisson brackets are defined as: $[f, g] = \partial_x f \partial_y g - \partial_x g \partial_y f$, where x and y are the coordinates in the "radial" and "poloidal" direction respectively. With this convention, $\mathbf{B} \cdot \nabla f = \nabla_\parallel f = [f, \psi] + \partial_z f$, and $\mathbf{V} \cdot \nabla f = [\phi, f]$. In all the equations above, the coordinates are normalized with respect to a typical equilibrium length scale, L, and the time with respect to the Alfvén time: $\tau_A = L/v_A$. Here, $v_A = B_z/\sqrt{4\pi m_i n_c}$ is the Alfvén velocity, with n_c a typical density and m_i the ion mass. The fields are normalized in such a way that only two dimensionless parameters are present in 1-3: the collisionless electron skin depth, $d_e = c/(\omega_{pe} L)$, and the ion sound Larmor radius, $\rho = \rho_s/L = c_s/(\Omega L)$. In our notation, c is the speed of light, $c_s = \sqrt{T_e/m_i}$ is the sound speed calculated with the electron temperature, $\omega_{pe} = e\sqrt{4\pi n_c/m_e}$ is the electron plasma frequency and $\Omega = eB_z/(m_i c)$ is the ion gyrofrequency. Finally, we define $\beta = 4\pi n_c T_e/B_z^2$.

It is appropriate to remark that the cold ion fluid description presented here is strictly valid only for $T_i \ll T_e$. In the presence of warm ions, the equations would need to be corrected with gyrofluid contributions. Our calculation therefore presents

an implicit quantitative imprecision for small wave length, although we expect that a more rigorous approximation would not radically change the qualitative behaviour of the system in the regimes investigated.

3. Primary and Secondary Instabilities

We take an equilibrium characterized by the absence of flows ($\phi_{eq} = 0$), with constant density gradients in the "radial" direction ($n_{eq} = -\widehat{v}_* x$) and with an homogeneous magnetic field in the "poloidal" direction ($\psi_{eq} = -B_p x$). Here $\widehat{v}_* = v_*/v_A$ and B_p are constants, the former representing the electron diamagnetic velocity, $v_* = -\frac{cT_e}{eB_z L_n}$, normalized to the Alfvén velocity (L_n is the length scale of the equilibrium density gradients). As shown below, the equilibrium affects the complex frequency of the instabilities (primary and secondary) only through the parameter $\Omega_* = (k_y v_*)/(k_\parallel v_A) = \sqrt{\beta}\frac{k_y \rho_s}{k_\parallel L_n}$, with $k_\parallel = \mathbf{k}\cdot\mathbf{B} = k_y B_p + k_z$. It is important to remark that Ω_* is a dimensionless number representing the ratio between the characteristic parallel and perpendicular time scale. This means that it is not just a simple redefinition of β, but rather a parameter that determines the relative importance of the Alfven and diamagnetic dynamics.

In our model, the pump (primary instability) is a wave in harmonic form: $\widetilde{\phi} = \Phi_0 e^{i\mathcal{A}} + \Phi_0^* e^{-i\mathcal{A}}$, where $\mathcal{A} = k_x x + k_y y + k_z z - \omega_0 t$ and the star symbol represents the complex conjugate. The perturbed fields $\widetilde{n}$ and $\widetilde{\psi}$ have a similar structure. The dispersion relation for this perturbation is obtained using the linearized version of the system 1-3:

$$(1-\Omega_0)(1-\Omega_*^2\Omega_0^2) - \Omega_0\mathcal{R}_\perp^2(1-\delta^2\Omega_0^2\Omega_*^2) = 0 \tag{4}$$

where $\Omega_0 = \omega_0/(\widehat{v}_* k_y)$, $\mathcal{R}_\perp = \rho k_\perp$, $\delta = d_e/\rho$ and $k_\perp^2 = k_x^2 + k_y^2$. The three solutions of this equation represent a Drift Wave (DW) coupled with two Kinetic Alfvén Waves (KAW). As the parameter Ω_* is increased, the standard electrostatic regime gives place to a regime in which the DW is strongly coupled with the KAWs and acquires an electromagnetic component. For Ω_* around unity, the DW replaces one of the KAW and vice versa, through a mode conversion process. Finally, we remark that $N_0 = (\Omega_0^{-1} - \mathcal{R}_\perp^2)\Phi_0$ and $\Psi_0 = \Omega_0\Omega_*\Phi_0$ complete the description of the pump (they will be needed in the derivation of the secondary instability).

The secondary instability, which occurs when the pump wave reaches a finite amplitude, is taken in the following form: $\widetilde{\phi} = \phi_s e^{i\mathcal{B}} + \phi_- e^{i(\mathcal{B}-\mathcal{A})} + \phi_+ e^{i(\mathcal{B}+\mathcal{A})} + c.c.$, with $\mathcal{B} = K_x x - \omega t$. This expression contains a zonal perturbation (first term on the RHS) and two sidebands (second and third terms on the RHS) [1]. The quantities K_x and ω are the radial wave number and the complex frequency of the zonal perturbation. Equations 1-3, linearized around an equilibrium that contains a finite amplitude pump wave, yield the growth rate of the secondary mode.

After some algebra, the system can be conveniently expressed through the matrix relation: $[M][U] = [0]$, with $[M]$ equal to:

$$\begin{bmatrix}
i\Omega & 0 & 0 & -I_-\widehat{\Phi}_0 & I_-\widehat{\Psi}_0 & 0 & I_+\widehat{\Phi}_0^* & -I_+\widehat{\Psi}_0^* & 0 \\
0 & i\Omega D_x & 0 & D_\perp\widehat{\Psi}_0 & \widehat{N}_0 - D_-\widehat{\Phi}_0 & -\widehat{\Psi}_0 & -D_\perp\widehat{\Psi}_0^* & -\widehat{N}_0^* + D_+\widehat{\Phi}_0^* & \widehat{\Psi}_0^* \\
0 & 0 & i\Omega & \widehat{N}_0 & -\mathcal{R}_x^2 I_-\widehat{\Psi}_0 & -\widehat{\Phi}_0 & -\widehat{N}_0^* & \mathcal{R}_x I_+\widehat{\Psi}_0^* & \widehat{\Phi}_0^* \\
\frac{\mathcal{R}_d^2}{\mathcal{R}_-^2}\widehat{\Phi}_0^* & -\frac{\mathcal{R}_d^2}{\mathcal{R}_-^2}\widehat{\Psi}_0^* & 0 & i\Omega_- & i\Omega_*^{-1} & 0 & 0 & 0 & 0 \\
-D_\perp\widehat{\Psi}_0^* & -(\widehat{N}_0^* - D_x\widehat{\Phi}_0^*) & \widehat{\Psi}_0^* & i\Omega_*^{-1} & i(\Omega_- D_- + 1) & -i\Omega_*^{-1} & 0 & 0 & 0 \\
-\widehat{N}_0^* & \mathcal{R}_d^2\widehat{\Psi}_0^* & \widehat{\Phi}_0^* & i & -i\mathcal{R}_-^2\Omega_*^{-1} & i\Omega_- & 0 & 0 & 0 \\
-\frac{\mathcal{R}_d^2}{\mathcal{R}_+^2}\widehat{\Phi}_0 & \frac{\mathcal{R}_d^2}{\mathcal{R}_+^2}\widehat{\Psi}_0 & 0 & 0 & 0 & 0 & i\Omega_+ & -i\Omega_*^{-1} & 0 \\
D_\perp\widehat{\Psi}_0 & \widehat{N}_0 - D_x\widehat{\Phi}_0 & -\widehat{\Psi}_0 & 0 & 0 & 0 & -i\Omega_*^{-1} & i[\Omega_+ D_+ - 1] & i\Omega_*^{-1} \\
\widehat{N}_0 & -\mathcal{R}_d^2\widehat{\Psi}_0 & -\widehat{\Phi}_0 & 0 & 0 & 0 & -i & i\mathcal{R}_+^2\Omega_*^{-1} & i\Omega_+
\end{bmatrix} \tag{5}$$

and $[U] = [\phi_s, \psi_s, n_s, \phi_-, \psi_-, n_-, \phi_+, \psi_+, n_+]^T$. We have defined $\Omega = \omega/(\widehat{v}_* k_y)$, $\Omega_\pm = \Omega \pm \Omega_0$, $\varepsilon = k_x/K_x$, $\widehat{\Phi}_0 = \Phi_0 K_x/\widehat{v}_*$ (same normalization for $\widehat{N}_0$ and $\widehat{\Psi}_0$), $\mathcal{R}_x = \rho K_x$, $I_\pm = (1 \pm 2\varepsilon)$, $\mathcal{R}_\pm^2 = \mathcal{R}_x^2 I_\pm + \mathcal{R}_\perp^2$, $\mathcal{R}_d^2 = \mathcal{R}_x^2 - \mathcal{R}_\perp^2$ and $D_a = (1 + \delta^2\mathcal{R}_a^2)$ with a standing for x, $\pm$ or $\perp$. The coefficients in 5 depend on six parameters: $\mathcal{R}_\perp$, δ, Ω_*, $\mathcal{R}_x$, ε and $\widehat{\Phi}_0$. The first three parameters directly affect the frequency of the pump (cf. 4), while the whole set determines the stability of the secondary instability, as its dispersion relation is given by the characteristic equation of the matrix. It can be easily proved that three of the nine roots of this equation correspond to $\Omega = 0$, while the other six can be obtained by solving the eigenvalue problem associated with the matrix, 5. If $\epsilon = 0$, the eigenvalues can be paired in three couples of complex conjugates.

4. Zonal perturbations in the Electromagnetic case

It is important to stress that in the presence of electromagnetic perturbations, the definition of a zonal perturbation is ambiguous. Indeed, it could refer to $k_y = k_z = 0$ perturbations in the original magnetic coordinates, $[\psi_{eq}(x), y, z]$, or in those perturbed by the pump, $[\psi(x, y, z), y, z]$. We adopt the former definition, which corresponds to assume that the pump does not change the flux surfaces too much, i.e. the quenching of the actual cross-field and of the old "radial" transport are similar.

While for weak primary instabilities the choice of one definition or the other does not significantly affect the understanding of the zonal flows and density, it can be extremely misleading when it comes to the zonal fields. Indeed, using the second definition, zonal fields can only be generated if Ohm's law contains terms that violate the frozen-in law. An example of these terms are those proportional to d_e. Crucially, only the second definition is relevant when discussing the effect of the zonal fields on current driven instabilities such as the tearing modes, because these depend on $dJ/d\psi$ rather than dJ/dx.

Thus, the new terms proportional to δ qualitatively change the behaviour of the system. The generation of zonal fields in Refs.[6, 7] and in our reference case (see below) should therefore be considered as an artefact of the procedure, and carry much less practical weight that those obtained in the presence of electron inertia.

5. Reference Case and Comparison with the Theory

We start our discussion with a reference case, $\epsilon = \delta = 0$, driven by a DW pump (which becomes a KAW at high β [10]). Figures 1(a) and 1(c) show the growth rate, $\Im(\Omega_{max})$, and the rotation frequency, $\Re(\Omega_{max})$, of the most unstable secondary mode as a function of Ω_* for different values of $\mathcal{R}_x$. Here the features of the pump

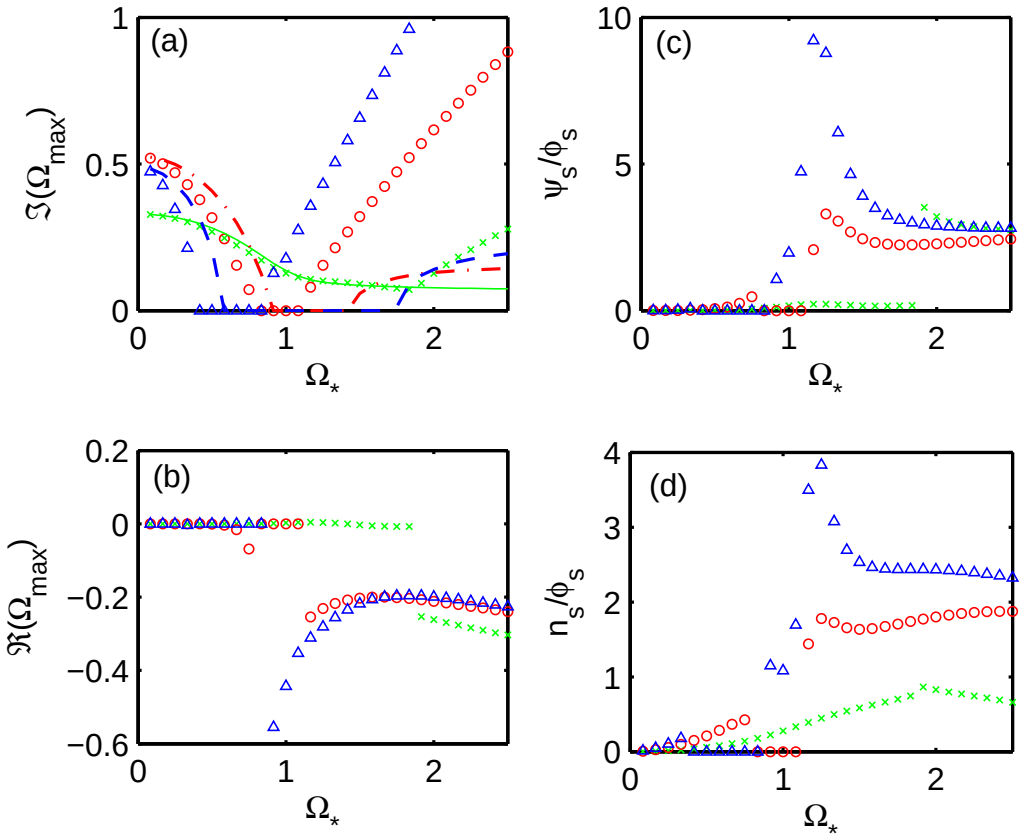

Figure 1. Growth rate (a), rotation frequency (b), ψ_s/ϕ_s (c) and n_s/ϕ_s (d) of the most unstable secondary mode as a function of Ω_*. Crosses, circles and triangles represent numerical solutions with $\mathcal{R}_x = 0.25, 0.5, 0.75$, respectively. The solid, dashed and dash-doted lines give a comparison with the theoretical prediction of [6]. Here $\delta = \epsilon = 0$, $\mathcal{R}_\perp = 0.25$ and $\widehat{\Phi}_0 = \mathcal{R}_x$.

(the background turbulence) are held fixed: $\mathcal{R}_\perp = 0.25$ and $\widehat{\Phi}_0 = \mathcal{R}_x$ (equivalent to $\Phi_0 e/T_e = \rho_s/L_n$ in dimensional units). The markers represent numerical solution of the eigenvalue problem associated with the matrix M ($\mathcal{R}_x = 0.25, 0.5, 0.75$ for crosses, circles and triangles, respectively). Figures 1(b) and 1(d) describe the amplitude of the zonal field, ψ_s, and of the zonal density, n_s, relative to the amplitude of the zonal flow, ϕ_s. As Ω_* approaches unity, both amplitudes are growing and become comparable to ϕ_s. The theoretical predictions of (10) in [6], shown in Figure 1(a) for comparison, are in reasonable agreement with the numerical data at extremely small Ω_* (i.e in the electrostatic limit) or $\mathcal{R}_x$. However, the theoretical model is not able to give a correct quantitative description of the branches of the secondary instability that appear at medium and large Ω_*, with errors well above 100% [see the bottom right part of Fig.1(a)]. Furthermore, the roots of (10) in [6] can only be purely real or purely imaginary, while our results clearly show that the eigenvalue is in general a complex number, the real part of which is significant for $\Omega_* \sim 1$ (i.e. in the electromagnetic regime).

This disagreement can be explained by noting that, given a generic matrix A as a function of a parameter λ, the determinant of the series expansion in λ of A equals the series expansion in λ of the determinant of A if, and only if, both series are truncated at the same order. That is:

$$\begin{aligned} det[A_{i,j}(\lambda)] &= det[A_{i,j}^{(0)} + A_{i,j}^{(1)}\lambda + \cdots + A_{i,j}^{(n)}\lambda^n + O(\lambda^{n+1})] \\ &= D^{(0)} + D(1)\lambda + \cdots + D(n)\lambda^n + O(\lambda^{n+1}). \end{aligned} \quad (6)$$

The calculation presented in [6, 7] is equivalent to a reduction (by substitution of variables) of the matrix M, 5, to a 4×4 matrix, the coefficients of which contain terms of order Ω^3. The coefficients of this matrix are then expanded and their series are truncated at order Ω but the determinant (the dispersion relation) is evaluated at order Ω^2, thus missing several relevant order terms as a consequence of the fact that the rule (6) is not respected. Furthermore, [6, 7] assume $n_s = 0$, which is not an acceptable approximation, as Figure 1(d) shows. The correct expansion would produce an extremely lengthy and complicated dispersion relation which could not provide clear insights. As a consequence, in this paper, we focus on an extensive numerical characterization of the system.

It is interesting to note that the finite real part of Ω_{max} which we obtain corresponds to a radial shift of the zonal structure and therefore of the velocity shear associated to it. If the time scale of this displacement is comparable or faster than an eddy turnover time, the zonal flow is less effective in quenching the turbulence [11]. This is due to the fact that the velocity shear pattern moves away before it is able to decorrelate the turbulent structure. In our model, we estimate the eddy turnover time as $\tau_{eddy} \approx L_n/c_s$, which implies that the effect of the zonal flows is significantly reduced if $|\Re(\Omega_{max})| \sim (k_y\rho_s)^{-1}$. In our calculation both $(k_y\rho_s)$ and $|\Re(\Omega_{max})|$ are smaller than unity [see Fig.1(c)], hence the radial motion of the zonal pattern is not sufficiently fast to lose effectiveness in quenching turbulence.

Figure 2 describes the stability of the system as the dimensionless parameters are varied. While at large $\mathcal{R}_\perp$ the secondary perturbation is generally growing, at smaller $\mathcal{R}_\perp$ two separated regions of instability can be identified. One corresponds to the electrostatic branch, which occurs at small Ω_* and for which ψ_s/ϕ_s is small. On this branch, increasing Ω_* reduces the growth rate of the instability. The opposite behaviour, which leads to positive feedback on the pressure and transport barrier formation [6], is observed in the second region, located at large Ω_* and $\mathcal{R}_x$. Here the perturbation is electromagnetic, i.e. ψ_s/ϕ_s is significant (and so is n_s/ϕ_s), see also Figure 1(c)-(d). We find that on this branch $\Im(\Omega_{max})$ grows indefinitely as $\mathcal{R}_x$ is increased (approximatively as $\mathcal{R}_x^2$). If sufficiently strong dissipative mechanisms are taken into account, the growth rate eventually reaches a maximum for a certain $\mathcal{R}_x$ and then decreases toward zero. If the maximum is at $\mathcal{R}_x$ larger than unity, the calculation would require kinetic corrections. In any case, within our model this prevents a clear identification of the maximum $\Im(\Omega_{max})$ (with respect to $\mathcal{R}_x$) as a function of Ω_* [6, 7, 12].

Figure 2 also shows that the electromagnetic branch can be destabilized only if Ω_* exceeds a value which roughly corresponds to $\beta \gtrsim (k_\parallel L_n)^2$. This condition is typically hard to achieve in the whole plasma by just increasing the pressure (i.e. β). Indeed, $k_\parallel = (qn - m)/(qR)$ and if L_n is of the order of the minor radius, a β larger than 5%-10% would be required (q is the safety factor, R the major radius, m and n the poloidal and toroidal mode numbers). On the other hand, close to a resonant surface where $q = m/n$ all the perturbations with the right helicity have

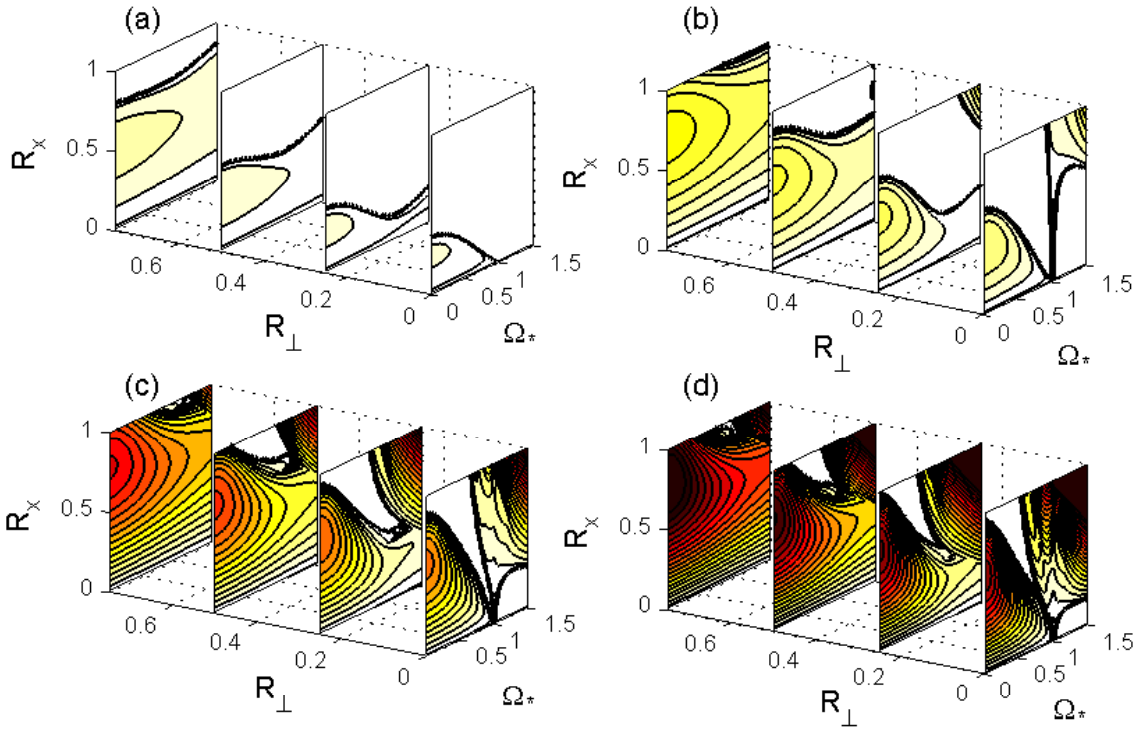

Figure 2. Isocontours of $\Im(\Omega_{max})$ as a function of $\mathcal{R}_x$, $\mathcal{R}_\perp$, Ω_* and $\widehat{\Phi}_0 = C_\Phi \mathcal{R}_x$ with $C_\Phi = 0.25$ (a), $C_\Phi = 0.5$ (b), $C_\Phi = 1$ (c) and $C_\Phi = 1.5$ (d). The thick black lines mark $\Im(\Omega_{max}) = 0$, within them $\Im(\Omega_{max}) > 0$ and the darker color in (d) corresponds to $\Im(\Omega_{max}) = 1$. $\delta = \epsilon = 0$.

vanishing parallel wave number (i.e. $k_\parallel \approx 0$) so that the threshold is easily exceeded, even at low β. It is important to remark that in standard toroidal configurations, the energy of the turbulence mostly resides in modes characterised by parallel wave numbers spanning from almost zero to once or twice $1/qR$ [13]. In particular, it is the ballooning nature of the instabilities that makes $k_\parallel \sim 1/qR$ a good approximation. However, at low shear the nature of the fluctuations changes and slab-like, $k_\parallel \approx 0$, modes can appear [14, 15]. In addition, electromagnetic instabilities like the micro-tearing modes naturally show a weak ballooning behaviour even in the presence of finite shear [16]. All these slab-like modes can provide at their resonant surface an effective drive for the zonal perturbation. As a consequence, the model described here could explain the generation of a transport barrier around low shear resonance surfaces (as measured experimentally, see [17]), where zonal flows and fields are stronger. Despite the simplicity of our argument, this interpretation was not present in previous similar works which approximated $k_\parallel \approx 1/qR$, therefore missing the resonant effect.

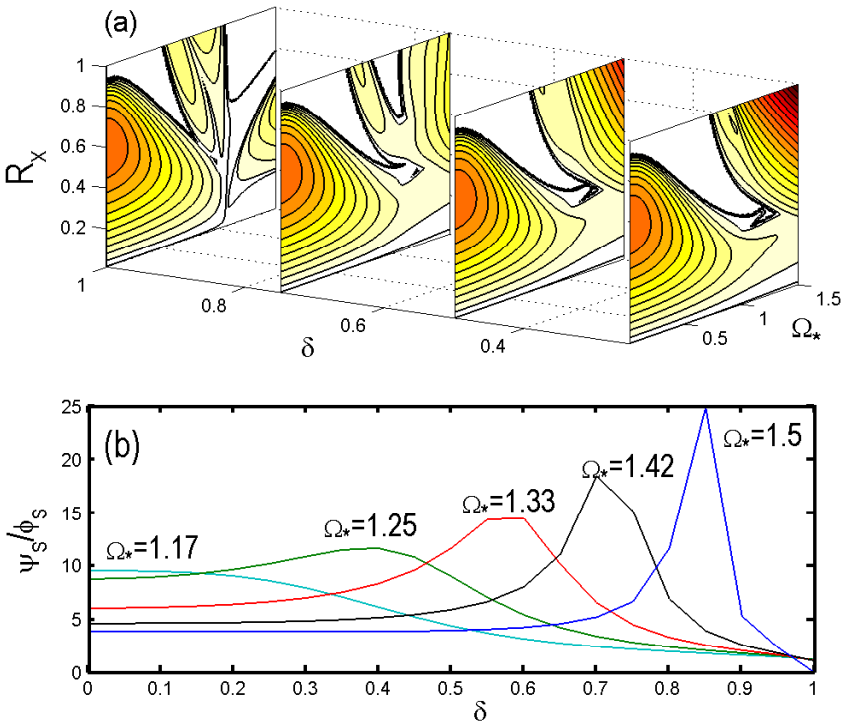

Figure 3. (a): Isocontours of $\Im(\Omega_{max})$ as a function of $\mathcal{R}_x$, δ, Ω_*. (b): ψ_s/ϕ_s as a function of δ for different values of Ω_* with $\widehat{\Phi}_0 = \mathcal{R}_x$, $\mathcal{R}_\perp = 0.25$, $\mathcal{R}_x = 0.75$ and $\epsilon = 0$.

6. Finite Electron Inertia and inhomogeneous Pump

We now move to the description of the effect of finite electron inertia, $\delta \neq 0$ ($\delta = 0.25 \div 0.75$ can be reached in experimental machines). As Figure 3(a) shows, the electrostatic branch is not significantly affected by a finite value of δ [cf. Figure 2(c)]. However, the electromagnetic branch bifurcates and is damped when δ approaches unity. Unfortunately, this means that the $\delta = 0$ estimate of the critical Ω_* for the formation of a transport barrier is underestimated. On the other hand, for finite δ the relative amplitude of the zonal field (and density) can become quite large, although its maximum shifts at higher values of Ω_* [see Figure 3(b)]. This is of great importance, since it suggests that zonal perturbations in the proper sense (see Section 4) are indeed generated and can affect the slope of the current density, $dJ/d\psi$.

So far we have considered cases in which the pump is a plain wave, $k_x = 0$, e.g. elongated streamers. We consider now localized eddies so that the scale of the zonal perturbation is intermediate between the equilibrium and the turbulence, $k_x > K_x > 1$. In Figure 4 we show how the growth rate of the perturbation varies for different ϵ (with $\widehat{\Phi}_0 = \mathcal{R}_x$, $\mathcal{R}_\perp = 1$, $\delta = 0$). We first remark that when $\epsilon > 1$ the parameter space is limited by the reality condition on k_y (i.e. $k_y^2 \geq 0$), which implies that $\mathcal{R}_x \leq \mathcal{R}_\perp/\epsilon$. As a consequence, only the part of Figure 4(c)-(d) below the horizontal line is meaningful. A radially inhomogeneous pump has two main effects:

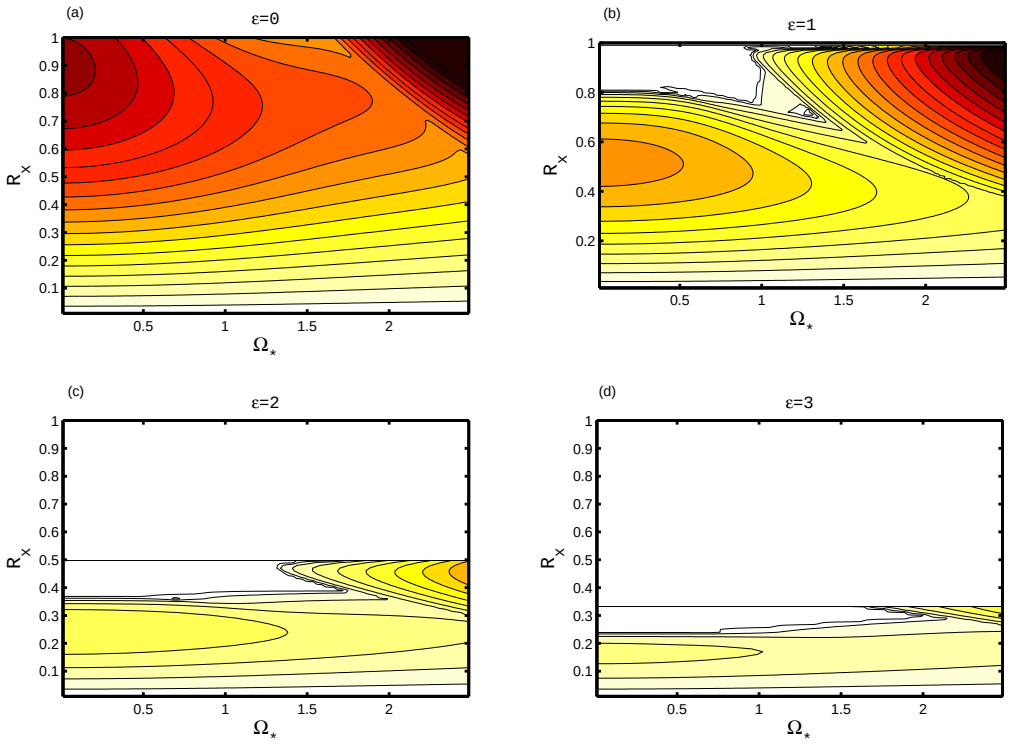

Figure 4. Isocontours of $\Im(\Omega_{max})$ as a function of $\mathcal{R}_x$ and Ω_* for (a) $\epsilon = 0$, (b) $\epsilon = 1$, (c) $\epsilon = 2$, (d) $\epsilon = 3$. In all the cases $\widehat{\Phi}_0 = \mathcal{R}_x$, $\mathcal{R}_\perp = 1$, $\delta = 0$.

it reduces $\Im(\Omega_{max})$ and it compresses the growth rate diagram in the $\mathcal{R}_x$ direction. However, an electrostatic and an electromagnetic branch a still present, although the excitation of the latter is pushed to larger values of Ω_*. We therefore find that small ϵ pumps are more effective in driving the zonal perturbation. This observation is in agreement with previous electrostatic results obtained with both Cheney-Hasegawa-Wakatani models and ETG simulations [18], where radially elongated fluctuations were shown to favour the generation of zonal structures. We remark, however, that our calculation only describes the onset of the zonal perturbation, not its fully nonlinear phase, in which the slower growing modes (large ϵ) could dominate the spectrum.

7. Criterion for ITB formation

Despite the fact that the results presented in the previous sections were obtained in different parametric regimes, we notice that the zonal flows are self-sustained if the local Ω_* exceeds a threshold value of order unity. In the regions of the plasma where this critical condition is met, intense velocity shear is therefore generated. If the region is large enough, this is likely to lead to local turbulent suppression and improved confinement. Starting from these considerations, in this section we apply the zonal flow theory presented above to construct a criterion for the formation of an internal transport barrier.

In the proximity of a resonant surface, located at a radius r_s, the parallel

wave number can be Taylor expanded, so that: $k_\parallel = \frac{qn-m}{qR} \cong s\frac{n}{R}\frac{x}{r_s}$, where $s = [r_s q'(r_s)]/q(r_s)$ is the magnetic shear and $x = r - r_s$. We remark that this step introduces an extrapolation of our theory since the calculations described in the previous sections assumed constant $k_\parallel$. Recalling that $\Omega_* = \sqrt{\beta}\frac{k_y\rho_s}{k_\parallel L_n}$, we can estimate the width of the region where the zonal perturbations are unstable: $x_{cr} \equiv r_s k_y \rho_s \frac{\sqrt{\beta}}{ns}\frac{R}{L_n}$. We now assume that the transport barrier forms if this width is larger than ρ_s, which represents the typical length scale of the turbulent eddies. In other words, this assumption means that the transport can be locally reduced only if the shearing associated with the zonal flows is generated over a region large enough to contain several turbulent eddies.

The condition $x_{cr} \gtrsim \rho_s$ is equivalent to:

$$\rho_{*M} \equiv \left(\frac{R}{d_i}\frac{q}{s}\right)\frac{\rho_s}{L_n} \equiv \frac{\sqrt{\beta}}{a/R}\frac{a}{L_n}\frac{q}{s} \gtrsim 1, \tag{7}$$

where $d_i = c/\omega_{ci}$ is the ion collisionless skin depth (which depends only on the plasma density) and a is the minor radius and we have used $k_y = m/r_s$. The left-hand side of the relation above implies that the formation of a transport barrier is facilitated by a low magnetic shear and by large ρ_s/L_n, as experimentally observed [19]. We note that the factor $qR/(sd_i)$ is roughly constant for machines with similar density, size and magnetic geometry.

It is useful to test this criterion to see if it can provide a qualitative prediction for the existence of transport barriers in typical plasmas. In order to do this we have to assume a profile for the density and for the safety factor. For the former we take $n/n(0) = (1 - \widehat{r}^4)$, where $\widehat{r} = r/a$, and for the latter we study three polynomial configurations: (I) standard with $q = 1 + 2\widehat{r}^2$; (II) hybrid, with low shear in the core, $q = 1 + 2r^5$; (III) reversed, with negative shear in the core, $q = 1 - \widehat{r}^2 - \widehat{r}^3 + 4\widehat{r}^4$. These profiles are shown in Fig.5

If we now take a typical fusion plasma, characterized by $\sqrt{\beta}/(a/R) = 0.3$, we find that in the core region the criterion is never satisfied for a standard profile, while a barrier is formed if the shear is low or in the case of a reversed q profile (see Fig.6). We note that in the latter case, the barrier forms in the neighbourhood of the position where the safety factor profile reaches its minimum, in agreement with experiment. If the shear is low, the barrier forms in the innermost part of the plasma, likely to be where a low n resonant surface lies. It is important to remark that the theory we developed is expected to fail in the edge region, since there the turbulence is highly nonlinear as a consequence of the steepness of the gradients and therefore our simple quasilinear treatment would not be valid. Hence, the rightmost part of the plots in Fig.6 cannot be used to predict barrier formation and should not be interpreted as an indication of pedestal formation.

Note that the criterion 7 is a necessary condition for the formation of the barrier, but it is not sufficient. Indeed, it only ensures that zonal perturbations are linearly unstable, but it does not say anything about their nonlinear evolution and saturation, which could eventually lead to the ITB. It is reasonable to expect that the barrier is produced when a sufficient amount of energy is transferred from the turbulence to the zonal perturbations. Our theory predicts that only the turbulent modes that resonate within the plasma can contribute to the generation of the zonal flows. As a consequence, when a new resonant surface enters the plasma, it carries a number of modes that can add up and strengthen the transport barrier. It is important to notice

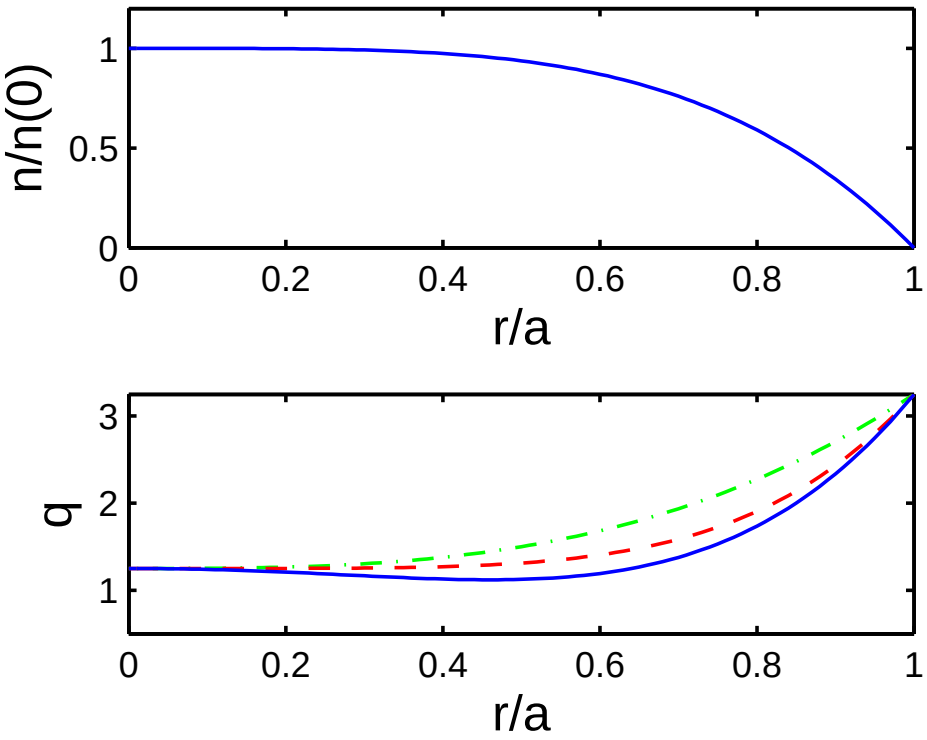

Figure 5. (a) Density and (b) safety factor profiles for case (I) dash-dot line, (II) dash line and (III) solid line.

that the low order rational surfaces have a special role in this mechanism since not all the resonances are equivalent.

To clarify this concept it is useful to assume that the turbulent fluctuations present in the plasma can be decomposed into N^2 modes represented by the couple $[m, n]$, where m and n are integer wave numbers that run from 1 to N. The modes with the same helicity, $h = m/n$, are a equivalence class and each helicity has N_h modes associated to it. We define $\mathcal{N}_h = N_h/N$, the density of the modes corresponding to h, and we plot this quantity as a function of h in Fig.7. This figure does not depend on the choice of N as long as it is sufficiently large. When a rational surface associated with a certain $q = q_0$ appears in the plasma the primary modes with helicity $h = q_0$ begin to resonate and some of them can destabilize new zonal modes. The low order resonant helicities, however, are more efficient at this because they have a much higher N_h and therefore their contribution is more important. Experimental studies [8] have indeed reported that the presence of these resonances is related to the triggering mechanism of the Internal Transport Barriers. From these considerations, we argue that in order to have a fully developed ITB two conditions should be met: the first is the validity of condition 7 and the second is the presence of a sufficient number of resonant modes (i.e. a q profile possessing low order rational surfaces).

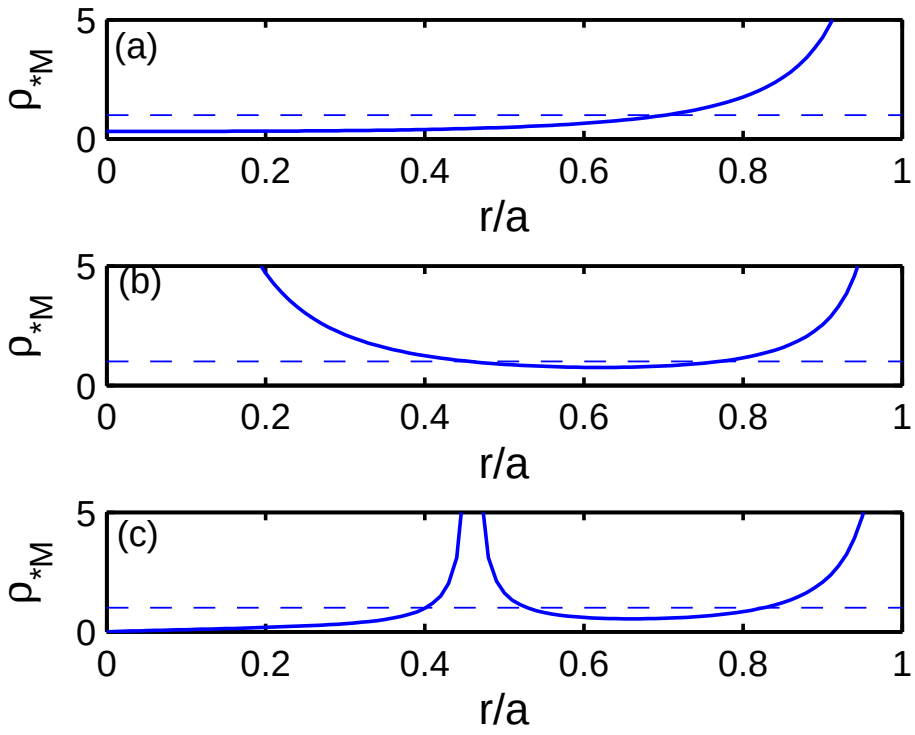

Figure 6. Value of ρ_{*M} (see Eq.7) as a function of the normalized radius for (a) the standard, (b) hybrid and (c) reversed safety factor in a typical configuration. The dashed line represents the approximative threshold above which the barrier is formed.

8. Conclusions

In conclusion, we have carried out a detailed study of the generation of zonal perturbations in the density, electric and magnetic field, considered as secondary instabilities arising in a turbulent Drift Wave bath. Our numerical study has exposed the weaknesses of the theoretical approaches and has shed some light on the new physics occurring when finite electron inertia and radial structure of the primary instability are taken into account. Our new results consistently show that the β threshold for the destabilization of the zonal flows is higher than the previous theoretical estimates. On the other hand, we have observed that low shear resonant surfaces play an important role in the generation of zonal perturbations, a feature that previous similar calculations failed to recognize. Only in these special locations, the magnitude of the zonal field and density can become significant and, at the same time, a pressure increase could trigger a feedback mechanism leading to transport barriers. It is important to remark that this mechanism is likely to work only for the ITBs in the plasma core. Indeed, at the pedestal in the plasma edge our quasilinear treatment is questionable since it was convincingly shown that fully developed edge turbulence does not carry any resemblance of the linear structures [20, 21] (i.e. our primary instability is not appropriate). As a consequence, neither the theory studied here

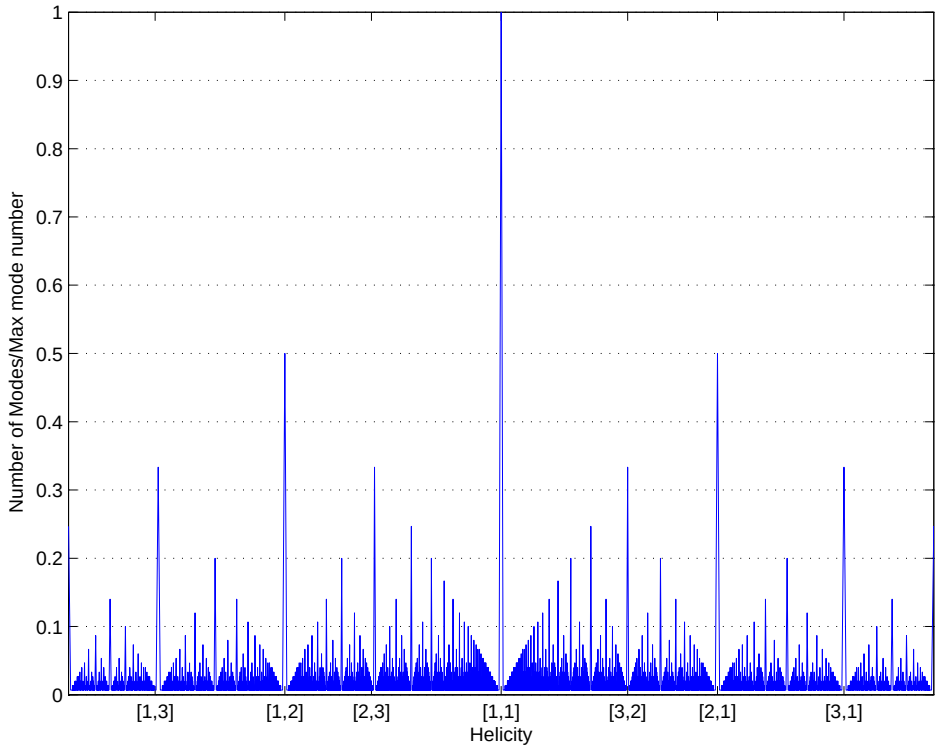

Figure 7. Mode density $\mathcal{N}_h$ as a function of the helicity.

nor those developed previously [6, 7, 5] can confidently predict L-H transition. The association between rational surfaces and zonal fields also suggests the possibility that magnetic islands could arise as a consequence of the local change of $dJ/d\psi$ occurring when $\delta \neq 0$ (see [22]). This could lead to a complex exchange of energy between the turbulence (microinstabilities), the zonal perturbations (mesoinstabilities) and MHD phenomena (macroinstabilities) and potentially reinforce the transport barrier [23].

Finally, in the light of the zonal flow description presented above, we have proposed a theoretical interpretation of the reason why ITB form around low order resonant surfaces. Our model predicts that the zonal flows are easily destabilized around rational surfaces even at low β. However, in order to have robust shear flows that can tear the eddies apart, the transition parameter Ω_* has to cross a critical threshold in a sufficiently large region around the resonant surface (of the order of the turbulence correlation length). In order to do that, the magnetic shear has to be low. Furthermore, low order rational surfaces are favoured in this process since in these locations a larger number of modes resonates and therefore can transfer their energy from the turbulence to the zonal perturbations.

Acknowledgments

The authors acknowledge illuminating discussions with Dr. A. Thyagaraja, Dr. P. de Vries and Prof. S. Cowley. This work was funded by the United Kingdom Engineering and Physical Sciences Research Council under grant EP/G003955 and the European

Communities under the contract of Association between EURATOM and CCFE. The views and opinions expressed herein do not necessarily reflect those of the European Commission.

[1] P.H. Diamond *et al* , Plasma Phys. Control. Fusion, 47, R35R161 (2005).
[2] A. Fujizawa *et al* , Phys. Rev. Lett., 98, 165001 (2007).
[3] A. Thyagaraja *et al* , Phys. Plasmas, 12, 090907 (2005)
[4] R.E. Waltz *et al* , Phys. Plasmas, 13, 052301 (2006)
[5] L. Chen *et al* , Nucl. Fusion, 41, 747 (2001).
[6] P.N. Guzdar *et al* , Phys. Rev. Lett., 87, 015001-1 (2001).
[7] P.N. Guzdar *et al* , Phys. Plasmas, 8, 3907 (2001).
[8] P.C. de Vries, E. Joffrin, M. Brix *et al.*, Nucl. Fusion, 49, 075007 (2009).
[9] R. Hazeltine *et al* , *Phys. Fluids* **28**, 2466 (1985).
[10] B.B. Kadomtsev, Plasma Turbulence (Academic, New York, 1965).
[11] T.S. Hahm, M.A. Beer, Z. Lin *et al* Phys. Plasmas, 6, 922 (1999).
[12] P.N. Guzdar *et al* , Phys. Plasmas, 11, 1109 (2004).
[13] T.T. Ribeiro and B Scott, Plasma Phys. Control. Fusion **47**, 16571679 (2005)
[14] F. Romanelli and F. Zonca, Phys. Fluids B **5**, 4081 (1993).
[15] J.W. Connor and R.J. Hastie Plasma Phys. Control. Fusion **46**, 1501 (2004).
[16] D.J. Applegate, C.M. Roach, J.W. Connor *et al* , Plasma Phys. Control. Fusion **49**, 11131128 (2007)
[17] R.C. Wolf, Plasma Phys. Control. Fusion **45**, R1 (2003).
[18] J.Q. Li, Y. Kishimoto, N. Miyato, T. Matsumoto and J.Q. Dong Nucl. Fusion **45**, 12931301 (2005).
[19] G. Tresset *et al.*, Nucl. Fusion, 42, 520 (2002).
[20] B.D Scott, New J. Phys. **4**, 52.1 (2002).
[21] B.D Scott, Phys. Plasmas **12**, 062314 (2005).
[22] F. Militello *et al* , *Phys. Plasmas* **16**, 032101 (2009).
[23] E. Joffrin, C.D. Challis, T.C. Hender *et al* , *Nucl. Fusion* **42**, 235 (2002).